CHAPTER 2 LITERATURE REVIEW

2.1 INTRODUCTION

In the past few decades, modal analysis has been a fast developing technique in the experimental evaluation of the dynamic properties of both mechanical systems and civil engineering structures. It has served a wide range of objectives such as identification and evaluation of vibration phenomena, validation, correction and updating of analytical dynamic models, development of experimentally based dynamic models, structural integrity assessment, structural modification and damage detection, establishment of criteria and specifications for design, test, qualification and certification. In recent years, many damage identification and updating methods have been proposed and this chapter presents a review of the current literature. In addition, this chapter presents some work done on the effect of boundary conditions on dynamic properties.

2.2 BOUNDARY CONDITIONS

In many cases, laboratory modal testing for beams are conducted under free-free or cantilever boundary conditions. However, in actual situations, most structures do not have these boundary conditions. Commonly, they are simply supported, fixed supported or combination of both boundary conditions. A change in boundary condition is one of the major factors influencing the dynamic properties of a structure.

In order to better understand the effect of a boundary condition, the classical theoretical approach is presented. According to Timoshenko et al. [1], the modal superposition technique is used to develop the transverse free vibration of beams with various boundary conditions. The beam displacement is expressed as a linear

combination of eigenfunctions or mode shapes. The typical normal function for transverse free vibrations of a prismatic beam is

$$X = C_1 \sin \lambda x + C_2 \cos \lambda x + C_3 \sinh \lambda x + C_4 \cosh \lambda x \qquad \text{Equation 2.1}$$

where the eigenvalue λ, and C_1, C_2, C_3 and C_4 are constants to be determined from each particular case of boundary condition.

2.2.1 SIMPLY SUPPORTED BEAM

The boundary conditions of a simply supported beam shown in Figure 2.1 are

$$(X)_{x=0} = 0 \qquad \text{Equation 2.2a}$$

$$(d^2X/dx^2)_{x=0} = 0 \qquad \text{Equation 2.2b}$$

$$(X)_{x=l} = 0 \qquad \text{Equation 2.2c}$$

$$(d^2X/dx^2)_{x=l} = 0 \qquad \text{Equation 2.2d}$$

which connote the fact that the displacement and the bending moment are zero at both end of the beam.

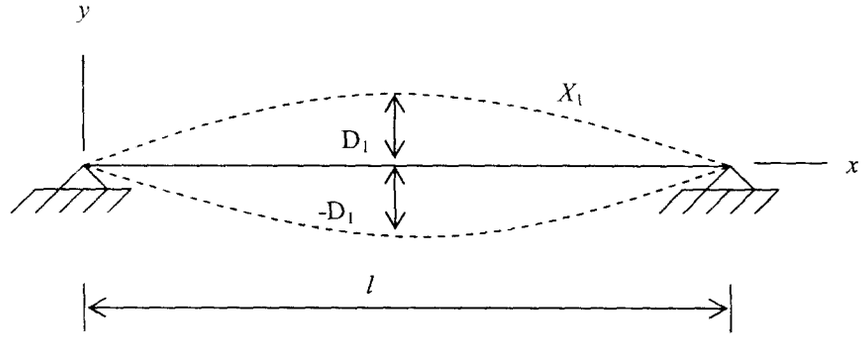

Figure 2.1 Timoshenko simply supported beam [1]

In order to solve Equation 2.1, it is useful to write the general expression for this normal function in the following form:

$$X = C_1(\cos \lambda x + \cosh \lambda x) + C_2(\cos \lambda x - \cosh \lambda x) +$$

$$C_3(\sin \lambda x + \sinh \lambda x) + C_4(\sin \lambda x - \sinh \lambda x) \qquad \text{Equation 2.3}$$

From Equations 2.2a and 2.2b, the constants C_1 and C_2 in Equation 2.3 must be equal to zero and from the Equations 2.2c and 2.2d, C_3 and C_4 are obtained in equal since $C_3 = C_4$ and

$$\sin \lambda l = 0 \qquad \text{Equation 2.4}$$

which is the frequency equation for the case under consideration. The non zero positive consecutive roots of Equation 2.4 are $\lambda_i l = i\pi$ for $i = 1, 2, 3 \ldots, \infty$. This frequency equation can be written as

$$\lambda_i = \frac{i\pi}{l} \qquad \text{Equation 2.5}$$

The deflected shape for various bending modes of vibration given by the normal function in Equation 2.3, with $C_1 = C_2 = 0$ and $C_3 = C_4 = D$, can be written as

$$X_i = D_i \sin kx = D_i \sin \frac{i\pi x}{l} \qquad \text{Equation 2.6}$$

where,

X_i is the deflection of the bending mode shape i,

i is the mode shape for $i = 1, 2, 3, \ldots, \infty$,

D_i is the amplitude of the mode shape i,

l is the span of the beam.

Thus, the bending mode shapes of a simply supported beam are in sine curves.

The angular frequencies corresponding to these λ_i values are obtained as

$$\omega_i = \lambda_i^2 \sqrt{\frac{EI}{\rho A}} = \frac{i^2\pi^2}{l^2} \sqrt{\frac{EI}{\rho A}} \qquad \text{Equation 2.7}$$

and the natural frequencies for corresponding bending mode shapes are

$$f_i = \frac{\omega_i}{2\pi} = \frac{i^2\pi}{2l^2} \sqrt{\frac{EI}{\rho A}} \qquad \text{Equation 2.8}$$

where $\sqrt{\frac{I}{A}}$ is the radius of gyration.

It is seen that the natural frequency of vibration for any mode is proportional to the radius of gyration of the cross section and inversely proportional to the square of the length.

2.2.2 FREE-FREE BEAM

The boundary conditions of free-free beams are

$$(dX/dx)_{x=0} = 0 \qquad \text{Equation 2.9a}$$

$$(d^2X/dx^2)_{x=0} = 0 \qquad \text{Equation 2.9b}$$

$$(dX/dx)_{x=l} = 0 \qquad \text{Equation 2.9c}$$

$$(d^2X/dx^2)_{x=l} = 0 \qquad \text{Equation 2.9d}$$

which connote the fact that the shear force and the bending moment are zero at both ends of the beam.

In order to satisfy Equation 2.3 for free-free condition, C_2 and C_4 must be equal to zero from Equations 2.9a and 2.9b, so that

$$X = C_1(\cos \lambda x + \cosh \lambda x) + C_3(\sin \lambda x + \sinh \lambda x) \qquad \text{Equation 2.10}$$

From Equations 2.9c and 2.9d,

$$C_1(-\cos \lambda l + \cosh \lambda l) + C_3(-\sin \lambda l + \sinh \lambda l) = 0 \qquad \text{Equation 2.11a}$$

$$C_1(\sin \lambda l + \sinh \lambda l) + C_3(-\cos \lambda l + \cosh \lambda l) = 0 \qquad \text{Equation 2.11b}$$

The solution of the constants C_1 and C_3, which is different from zero, can only be obtained in the case when the determinant of Equations 2.11a and 2.11b vanishes. In this manner the following frequency equation is obtained:

$$(-\cos \lambda l + \cosh \lambda l)^2 - (\sinh^2 \lambda l - \sin^2 \lambda l) = 0$$

$$\cos^2 \lambda l + \cosh^2 \lambda l - 2\cos \lambda l \cosh \lambda l - \sinh^2 \lambda l + \sin^2 \lambda l) = 0$$

$$\cos^2 \lambda l + \sinh^2 \lambda l + \cosh^2 \lambda l - \sinh^2 \lambda l - 2\cos \lambda l \cosh \lambda l = 0 \qquad \text{Equation 2.11c}$$

where,

$$\cos^2 \lambda l + \sinh^2 \lambda l = 1 \qquad \cosh^2 \lambda l - \sinh^2 \lambda l = 1$$

Hence, Equation 2.11c can be written as:

$$2 - 2\cos \lambda l \cosh \lambda l = 0$$

$$\cos \lambda l \cosh \lambda l = 1 \qquad \text{Equation 2.12}$$

By solving mathematically method, the consecutive roots of Equation 2.12 are

$\lambda_0 l$	$\lambda_1 l$	$\lambda_2 l$	$\lambda_3 l$	$\lambda_4 l$	$\lambda_5 l$	$\lambda_6 l$
0	4.73	7.853	10.966	14.137	17.279	23.5619

The nonzero roots can be formulated approximately as:

$$\lambda_i l \approx (i + \tfrac{1}{2})\pi \qquad \text{Equation 2.13}$$

The values of constants C_1 and C_3 varies for each bending mode of vibration, by substituting the consecutive roots of equation 2.12 for each corresponding bending mode, the ratio C_1/C_3 can be found. Then the deflection shape of each vibration mode can be obtained from Equation 2.10. Figures 2.2a, 2.2b and 2.2c presented the first three vibration modes for corresponding frequencies f_1, f_2 and f_3.

On these vibration modes, the rigid body displacements of the beam can be superimposed with the lower bending modes. This combined rigid body motion may be characterized as

$$X = c_1 + c_2 x \qquad \text{Equation 2.14}$$

This expression presents a translator displacement together with the rotation that can be superimposed on free vibration.

The natural frequencies for corresponding bending modes can be found by using Equation 2.7.

$$f_i = \frac{\omega_i}{2\pi} = \frac{(i+\tfrac{1}{2})^2 \pi}{2l^2}\sqrt{\frac{EI}{\rho A}} \qquad i \neq 0 \qquad \text{Equation 2.15}$$

It is generally believed that the higher the stiffness of the support, the higher will be the natural frequencies, when all other factors remain unchanged. However based on the above analytical observation on free-free and simply supported beams, the flexural

natural frequencies of free-free beams are higher than the natural frequencies of simply supported beam, as shown in equation 2.16.

$$f_{free} = \frac{(i+\frac{1}{2})^2 \pi}{2l^2}\sqrt{\frac{EI}{\rho A}} > f_{simply} = \frac{i^2\pi}{2l^2}\sqrt{\frac{EI}{\rho A}} \quad \text{if } i \neq 0 \qquad \text{Equation 2.16}$$

Moreover, Mostafiz [6] also found that the less the stiffness of the support of a uniform rectangular test plate, the higher the natural frequency.

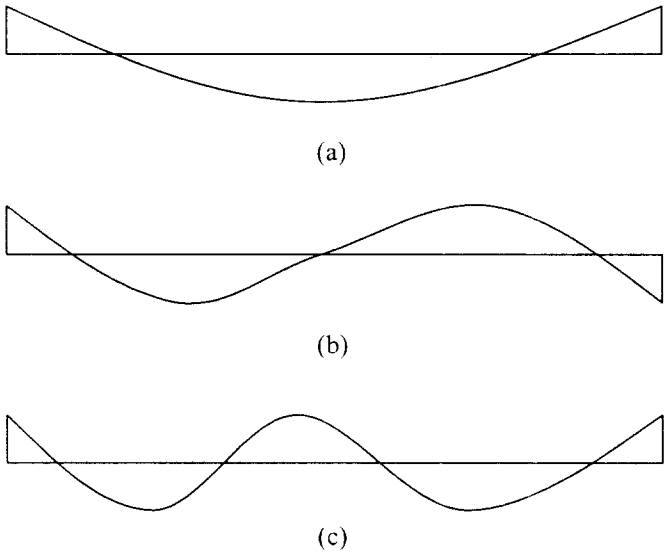

Figure 2.2 First three modes of vibration for free-free beam [1]

2.3 DAMAGE IDENTIFICATION METHODS

Current damage-detection methods are either visual or localized experimental methods such as ultrasonic, magnet field, radiograph, eddy-current and thermal field methods. All these are only capable of detecting damage on or near the surface of the structure. However, structures today have increased so much in complexity and size that global damage identification methods have to be applied to evaluate and diagnose their state of health. Modal analysis or vibration testing is a technique that is able to provide a global way of damage identification of a structure from the changes of its dynamic properties. The basic idea is that modal properties that is natural frequency, mode shape and modal damping, are functions of the physical properties of a structure in terms of its

mass, stiffness and damping. Therefore, changes in the physical properties will cause changes in the modal properties.

2.3.1 NATURAL FREQUENCY CHANGES

The natural frequency of a structure bears a direct relationship with the structural stiffness. For an undamped vibrating system with mass m, the relationship can be written as

$$\omega_i = \sqrt{\frac{EI}{m}} \qquad \text{Equation 2.17}$$

where EI is the stiffness and ω_i is the natural frequency for mode i of the system. Based on Equation 2.17, a reduction in stiffness EI of a structure leads to the reduction of the natural frequency for a corresponding mode. Thus the natural frequency of a vibrating system is a useful global parameter to indicate the occurrence of damage and to evaluate the severity or state of damage in a structure.

Cawley and Adams [2] pointed the fact that the stress distribution in a vibrating structure is non-uniform and each change in natural frequency is different to the corresponding mode shape. Any localized damage would affect each mode differently and the changes in natural frequencies depend on the particular location of the damage. Therefore, natural frequency changes are not only useful to monitor globally the structural health condition but is also able to identify the damage location, which is local in nature.

The degree of reduction in natural frequency is dependent on the position of the defect relative to the mode shape for a particular mode of vibration [2,3]. When the damage is located at the regions of high curvature of the mode shapes, the reduction of natural frequency becomes more significant [4]. Similar result was obtained from Narayana and Jebaraj [5], where the percentage change in natural frequency was

higher for the crack at high strain position than for the crack at low strain position. They proposed an energy concept to relate the natural frequency with the strain mode and directly used the natural frequencies to identify and locate the crack. The theoritical background and case study of Narayana and Jebaraj [5] work is presented herein.

The general equation for transverse free vibration in bending mode of a beam is

$$\frac{\partial^2}{\partial x^2}\left[EI\frac{\partial^2 y}{\partial x^2}\right]dx + \rho A\, dx\frac{\partial^2 y}{\partial t^2} = 0 \qquad \text{Equation 2.18}$$

By solving Equation 2.18, the natural frequency is

$$\omega^2 = \lambda = \frac{\int_0^l EI(x)\{d^2y/dx^2\}^2 dx}{\int_0^l md^2y\ dx} = \frac{U}{V} \qquad \text{Equation 2.19}$$

where,

$U = \frac{EI}{2}\int_0^l (d^2y/dx^2)dx$ is the strain energy.

$V = \frac{m}{2}\int_0^l d^2y\ dx$ is the kinetic energy.

Taking the variation of λ from Equation 2.18, then $\partial\lambda$ is

$$\partial\lambda = \frac{\partial U}{V} - \frac{U\partial V}{V^2} \qquad \text{Equation 2.20}$$

and divide $\partial\lambda$ with λ,

$$\frac{\partial\lambda}{\lambda} = \frac{\partial U}{U} - \frac{\partial V}{V} \qquad \text{Equation 2.21}$$

when there is only a small damage or crack on the beam, change in mass is very small, $\delta m = 0 \Rightarrow \delta V = 0$. So

$$\frac{\partial\lambda}{\lambda}=\frac{\partial U}{U}=\frac{E\partial\left[\int_0^l I\{d^2y/dx^2\}^2dx\right]}{E\int_0^l I\{d^2y/dx^2\}^2dx} \qquad \text{Equation 2.22}$$

By considering ∂U from Equation 2.22, and assuming the crack occur at l_0 with a crack width of Δx, ∂U can be written as

$$\partial U=\partial\left[\int_0^{l_0}EI\left\{\frac{d^2y}{dx^2}\right\}^2dx+\int_{l_0}^{l_0+\Delta x}EI\left\{\frac{d^2y}{dx^2}\right\}^2dx+\int_{l_0+\Delta x}^{l}EI\left\{\frac{d^2y}{dx^2}\right\}^2dx\right] \qquad \text{Equation 2.23}$$

Since the change in curvature is only significant at the crack location, the changes is from l_0 to $l_0 + \Delta x$. On the other hand, the change in curvature from 0 to l_0 and $l_0 + \Delta x$ to l of the above equation can be considered insignificant or zero. Then,

$$\partial U=\partial\left[0+\int_{l_0}^{l_0+\Delta x}EI\left\{\frac{d^2y}{dx^2}\right\}^2dx+0\right]$$

$$\partial U=E\left[\int_{l_0}^{l_0+\Delta x}\partial I\left\{\frac{d^2y}{dx^2}\right\}^2dx+\int_{l_0}^{l_0+\Delta x}I\cdot\partial\left\{\frac{d^2y}{dx^2}\right\}^2dx\right]$$

$$\partial U=EI\left[\frac{\partial I}{I}\int_{l_0}^{l_0+\Delta x}\left\{\frac{d^2y}{dx^2}\right\}^2dx+\int_{l_0}^{l_0+\Delta x}\partial\left\{\frac{d^2y}{dx^2}\right\}^2dx\right] \qquad \text{Equation 2.24}$$

Since the integration limit is for a small crack width of only Δx, Equations 2.24 and 2.22 can be written as

$$\partial U=EI\left[\frac{\partial I}{I}\left\{\frac{d^2y}{dx^2}\right\}^2\Delta x+\partial\left\{\frac{d^2y}{dx^2}\right\}^2\Delta x\right]$$

$$\partial U=EI\left\{\frac{d^2y}{dx^2}\right\}^2_{at\ldots l_0}\Delta x\left[\frac{\partial I}{I}+\frac{\partial\{d^2y/dx^2\}^2_{at\ldots l_0}}{\{d^2y/dx^2\}^2_{at\ldots l_0}}\right]$$

$$\frac{\partial\lambda}{\lambda}=\frac{\partial U}{U}=\frac{\{d^2y/dx^2\}^2_{at\ldots l_0}\Delta x\left[\frac{\partial I}{I}+\frac{\partial\{d^2y/dx^2\}^2_{at\ldots l_0}}{\{d^2y/dx^2\}^2_{at\ldots l_0}}\right]}{\int_0^l\{d^2y/dx^2\}^2dx} \qquad \text{Equation 2.25}$$

Equation 2.25 indicates that the variation of frequency parameter $\partial\lambda/\lambda$ is a function of square of transverse strain of the beam at the crack location. Also, it is a function of the variation of moment inertia, $\partial I/I$ and variation of the square of transverse strain at the crack location.

Equation 2.25 can also be applied to the free vibration in the torsional mode. This equation can be developed by replacing the displacement parameter, y and moment inertial in Equation 2.25 with the radian parameter, θ and torsional inertial, J.

$$\frac{\partial\lambda}{\lambda}=\frac{\partial U}{U}=\frac{\{d^2\theta/dx^2\}^2_{at\ldots l_0}\Delta x}{\int_0^l\{d^2\theta/dx^2\}^2dx}\left[\frac{\partial J}{J}+\frac{\partial\{d^2\theta/dx^2\}^2_{at\ldots l_0}}{\{d^2\theta/dx^2\}^2_{at\ldots l_0}}\right] \qquad \text{Equation 2.26}$$

The above equation indicates that the variation of frequency parameter $\partial\lambda/\lambda$ is a function of square of torsional strain of the beam at the crack location. Also it is a function of the variation of torsional inertia, $\partial J/J$ and of the squared torsional strain at the crack location. Thus, it indicates that change in natural frequency for flexural and torsional modes due to crack damage is non-linear.

Using Equations 2.25 and 2.26, graphs of the frequency changes are plotted against the length of a cantilever beam. These are shown in Figure 2.3 with normalized maximum value at the fixed end at unity. It was observed that the changes in natural frequencies were maximum if the crack was located at the peak or trough of the strain mode, and they were of minimum value if the crack location was at the node of the strain mode. The locations of peak or trough and node of the bending and torsional strain modes for the cantilever beam are listed in Table 2.1.

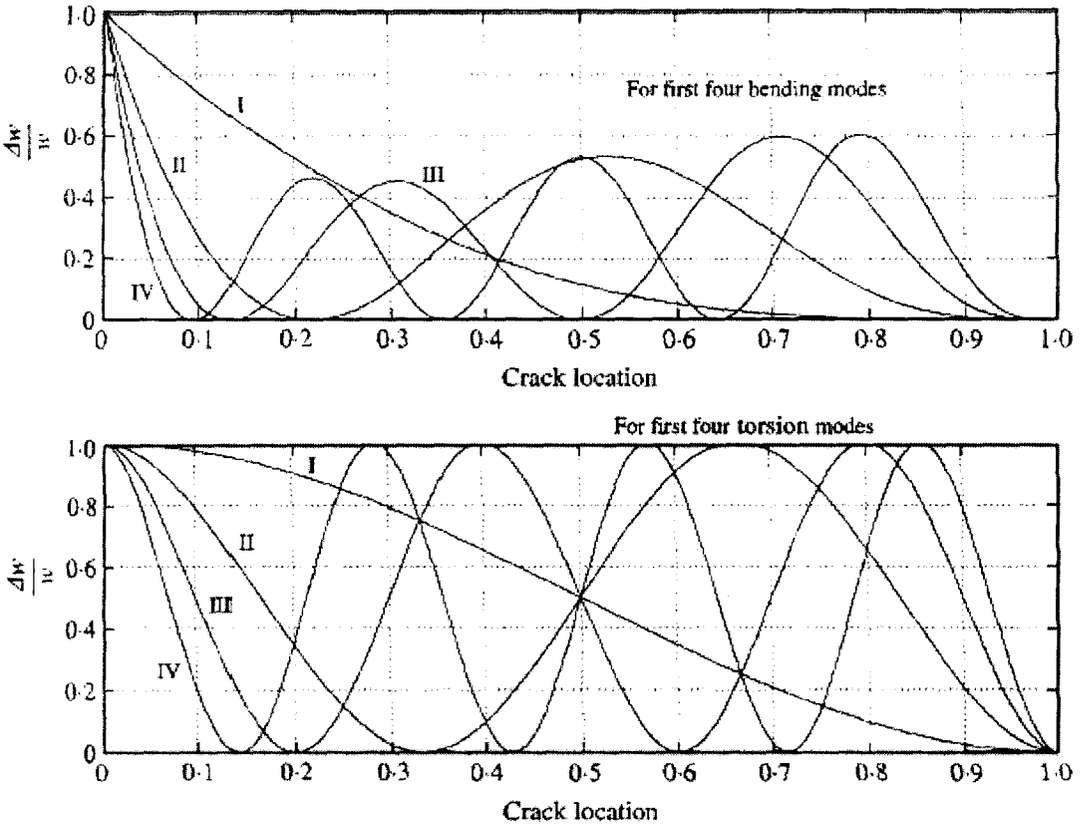

Figure 2.3 Change in frequency versus crack location of cantilever beam (first four bending and four torsional modes) [5]

Mode	Peak/trough locations	Node locations
Bending mode 1	0.0L	1.0L
Bending mode 2	0.0L, 0.5287L	0.2175L, 1.0L
Bending mode 3	0.0L, 0.3075L, 0.7087L	0.1325L, 0.4907L, 1.0L
Bending mode 4	0.0L, 0.22L, 0.5L, 0.795L	0.0945L, 0.356L, 0.6416L, 1.0L
Torsional mode 1	0.0L	1.0L
Torsional mode 2	0.0L, 0.6667L	0.3333L, 1.0L
Torsional mode 3	0.0L, 0.4L, 0.8L	0.2L, 0.6L, 1.0L
Torsional mode 4	0.0L, 0.285L, 0.5725L, 0.8775L	0.1425L, 0.4275L, 0.7125L, 1.0L

Table 2.1 Peak or trough and node locations of strain mode shapes for cantilever beam [5]

Referring to Table 2.1, there are seven peaks or trough and seven nodes for both strain modes. Therefore, the crack can be located in the vicinity of any one of the 28 locations, 14 locations from bending modes and 14 location from torsional modes. Thus

the accuracy of the prediction will be approximately L/28, and a case study was carried out on the cantilever beam.

From Table 2.2, the maximum percentage change in natural frequencies for the bending modes occurred for mode 3. Based on the observation from Table 2.1, it was observed that the possible crack location was at 0.0L (fixed end), 0.3075L or 0.7087L. The maximum percentage change in frequency for torsional modes occurred for mode 2 and the possible crack location would be at 0.0L or 0.6667L. The crack was not located near to the fixed end because the change in the first bending mode and torsional mode was much less. Therefore, the possible crack location was between 0.6667L and 0.7078L from the fixed end. The exact crack location was 0.67L for 50% crack depth. The predicted result matched closely the exact crack location.

Mode no.	Percentage change in frequencies	
	Bending modes	Torsional modes
1	0.1697	2.0114
2	3.1704	7.0786
3	4.2831	1.5722
4	1.9605	4.6405

Table 2.2 Percentage change in frequency due to crack [5]

2.3.2 ROTATIONAL SPRING MODEL

A crack in the beam can be modeled as a 'fracture hinge' concept or rotational spring model in which the spring stiffness represents the crack stiffness, k_t at the crack location [7,8,9]. The crack stiffness is constant for all vibration modes and the intersection point of the crack stiffness at various natural frequencies, ω_i, along the axial direction of the beam represent the possible crack location. In order to obtain good results, the minimum of three measurements of natural frequencies should be obtained experimentally.

In a study carried out by Boltezar et al. [7], the single crack beam was modeled into two segments of beam and the rotational spring was modeled as a crack between the two segments. The model is shown in Figure 2.4.

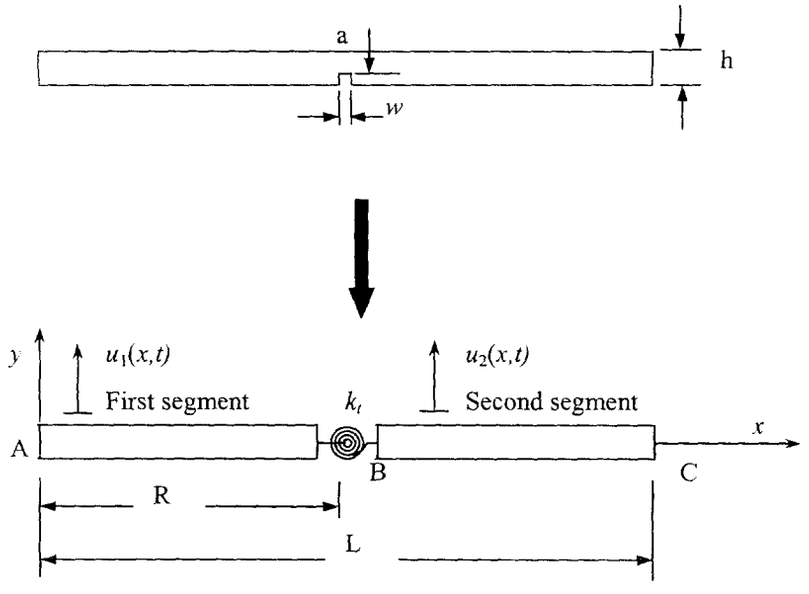

Figure 2.4 Model of the cracked free-free beam with rotational spring [7]

Displacement mode shape for both the segments is given in Equation 2.27 where u_1 and u_2 are displacements on the first and second segment.

$$u_{1B} = C_1 \sin \lambda x + C_2 \cos \lambda x + C_3 \sinh \lambda x + C_4 \cosh \lambda x$$

$$u_{2B} = D_1 \sin \lambda x + D_2 \cos \lambda x + D_3 \sinh \lambda x + D_4 \cosh \lambda x \qquad \text{Equation 2.27}$$

At the crack position B, the continuity condition requires equal displacements, moments and shear forces at both sides of a crack except the rotation.

$$u_{1B} = u_{2B} \qquad u''_{1B} = u''_{2B} \qquad u'''_{1B} = u'''_{2B} \qquad \text{Equation 2.28}$$

The rotation between two segments is related to the moment of each section and the crack stiffness k_t.

$$u'_{1B} + \frac{u''_{1B}}{k_t} = u'_{2B} \qquad \text{Equation 2.29}$$

Boundary and continuity conditions result in a set of 8 homogeneous linear algebraic equations for eight unknown coefficients. For a non-trivial solution, the determinant defined in Equation 2.30 must be zero. In the determinant of Equation 2.30, $\delta = k_t/EI$ denotes relative flexural stiffness that models the crack.

$$f(R,\lambda,\delta)=\begin{vmatrix} 0 & -1 & 0 & 1 & 0 & 0 & 0 & 0 \\ -1 & 0 & 1 & 0 & 0 & 0 & 0 & 0 \\ -\sin\lambda R & -\cos\lambda R & \sinh\lambda R & \cosh\lambda R & \sin\lambda R & \cos\lambda R & -\sinh\lambda R & -\cosh\lambda R \\ -\cos\lambda R & \sin\lambda R & \cosh\lambda R & \sinh\lambda R & \cos\lambda R & -\sin\lambda R & -\cosh\lambda R & -\sinh\lambda R \\ \cos\lambda R-\frac{\lambda}{\delta}\sin\lambda R & -\sin\lambda R-\frac{\lambda}{\delta}\cos\lambda R & \cosh\lambda R+\frac{\lambda}{\delta}\sinh\lambda R & \sinh\lambda R+\frac{\lambda}{\delta}\cosh\lambda R & -\cos\lambda R & \sin\lambda R & -\cosh\lambda R & -\sinh\lambda R \\ \sin\lambda R & \cos\lambda R & \sinh\lambda R & \cosh\lambda R & -\sin\lambda R & -\cos\lambda R & -\sinh\lambda R & -\cosh\lambda R \\ 0 & 0 & 0 & 0 & -\sin\lambda L & -\cos\lambda L & \sinh\lambda L & \cosh\lambda L \\ 0 & 0 & 0 & 0 & -\cos\lambda L & \sin\lambda L & \cosh\lambda L & \sinh\lambda L \end{vmatrix}=0$$

Equation 2.30

where,

$\delta = \dfrac{k_t}{EI}$ is relative stiffness at the crack position

$\lambda^4 = \dfrac{\rho A \omega^2}{EI}$ is the eigenvalue

In the procedure of identifying the crack location, firstly, the natural frequencies ω_i of flexural vibrations of the free-free beam were measured. Next, the eignevalues λ_i were computed using the measured natural frequencies and Young's modulus of the intact beam. Finally, the relative stiffness δ is computed from Equation 2.30 as a function of possible crack location for each of the natural frequencies and all of the frequencies were presented on the same graph as depicted in Figure 2.5. In the graph, the intersection of the relative stiffness value δ shows the possible crack location.

The results of free-free beam were plotted against the relative possible crack location R/L and are shown in Figure 2.5 for two different values of the relative crack depth, a/h, 11.3 and 36.3%. The true crack location was at R/L = 0.38 where the percentage difference with true crack location for both relative crack depths was less

than 1%. These results indicated that the rotational spring model provided high sensitivity and high accuracy in damage identification. However, to produce satisfactory results, the changes in natural frequencies must be measured with great accuracy. Furthermore, since the free-free beam is symmetrical, there will be two possible crack locations indicated but only one is correct.

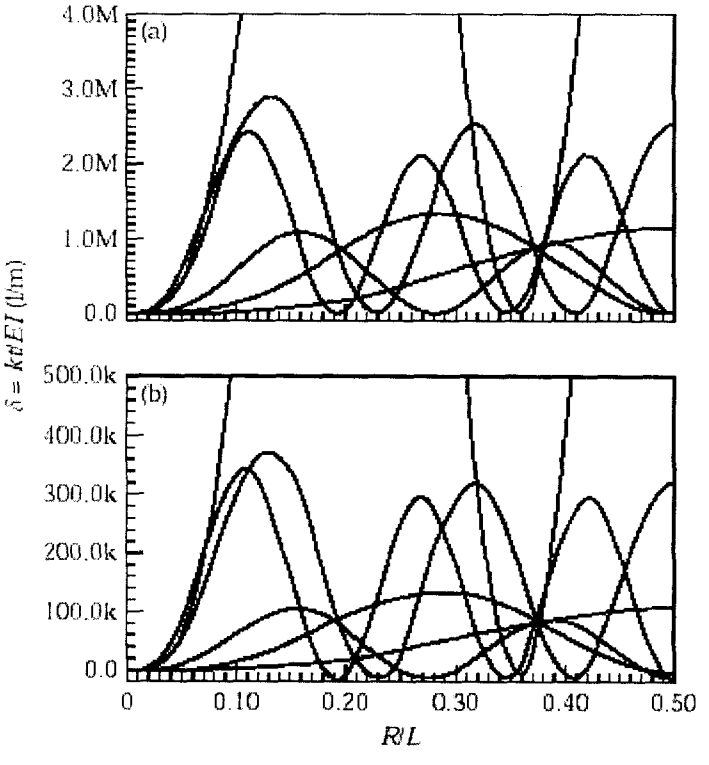

Figure 2.5 Relative crack stiffness versus crack location for the first 6 natural frequencies and for 2 different relative crack depths: (a) a/h = 11.3%; (b) a/h = 36.3% [7]

2.3.3 SENSITIVITY CONCEPT

The sensitivity concept is based on the premise that the ratio of changes in two natural frequencies is a function of the damage location $h(r)$, if changes in stiffness are independent of frequency [2].

$$\frac{\delta\omega_i}{\delta\omega_j} = h(r) \qquad \text{Equation 2.31}$$

Positions where the theoretically determined ratio of changes in two natural frequencies $\delta\omega_{xi}/\delta\omega_{xj}$ equals the experimentally measured value $\delta\omega_{xi}/\delta\omega_{xj}$ are therefore possible damage sites.

The ratio of changes in two theoretical natural frequencies due to the selected damage element is calculated using theoretical or finite element methods. The changes in theoretical natural frequencies are a function of the modal sensitivity [2]. Therefore, the ratio of measurement changes in natural frequencies also equals the ratio of theoretically measured sensitivities and can be written as

$$\frac{\delta\varpi_i}{\delta\varpi_j} = \frac{\delta\lambda_{ir}}{\delta\lambda_{jr}} \qquad \text{Equation 2.32}$$

where

$\frac{\delta\varpi_i}{\delta\varpi_j}$ is the measured ratio of changes in frequencies for two modes, i and j.

$\frac{\delta\lambda_{ir}}{\delta\lambda_{jr}}$ is the ratio of theoretically measured sensitivities for those modes and element r.

The theoretically measure sensitivity is

$$\delta\lambda = \frac{\phi^T \delta K \phi}{\phi^T M \phi} \qquad \text{Equation 2.33}$$

where δK is the change in stiffness due to damage at particular element in the structure, M is the element mass and ϕ is the eigenvector.

Equation 2.32 is true only when element r is exactly representing the crack on the test structure. So the error index is introduced as

$$e_r = \frac{\delta\varpi_i}{\delta\varpi_j} - \frac{\delta\lambda_{ir}}{\delta\lambda_{jr}} \qquad \text{Equation 2.34}$$

where e_r represents the localization error of element r and when $e_r = 0$ is an indication of the damage location.

Accuracy of sensitivity-based method is dependant on either the number of modes or the type of modes that are used in the calculation [10]. The quality of the finite element model or other theoretical model used to compute the sensitivities is also a factor determining the accuracy. This method is most useful for basic structures where the damage only affects one significant stiffness component in the structure [4].

2.3.4 MODE SHAPE

Mode shapes are inherent properties of a structure and they do not depend on the forces or load acting on the structure [11]. Changes in mode shapes depend on the material properties that is mass, stiffness and damping or boundary conditions of the structure. Mode shapes have no unique values, and hence no units associated with them. However, mode shapes are unique as it represent the motion of one point relative to another at resonance.

When a localized damage occurs, material properties in the structure are affected, hence stiffness changes around the damage area rather than the other areas changes. Since changes in mode shapes depend on the material properties, monitoring the changes gives a more direct and significant indication of the damage occurring in the structure.

2.3.4.1 MODE SHAPE DEVIATION

The change in displacement mode shapes at a particular point is related to the stiffness of a structure. A localized damage occurs when stiffness in the damaged area is affected more than other areas of the structure. Similarly, changes in displacement mode shapes at a damaged location are also affected compared to other locations. Pandey [12] used a finite element model of a simply supported beam to study the absolute mode shape deviation obtained by comparing the intact displacement mode shapes with the

damage displacement mode shapes at particular nodes. The absolute mode shape deviation can be written as

$$D_{in} = \left|\phi_{in}^{u} - \phi_{in}^{d}\right| \qquad \text{Equation 2.35}$$

where ϕ^{u} is the intact displacement mode shape and ϕ^{d} is the damage displacement mode shape at n node.

The deviation in displacement mode shapes was distributed throughout the span of the beam and the results are shown in Figure 2.6. It was apparent that the deviation was quite insignificant. In a paper written by Narayana [5], deviation in mode shape was not sufficient for indicating the location of the crack. A finite element cantilever beam was considered, with its low value of maximum deviation at the crack location compared to deviations at other locations throughout the span of beam. The differences were very small and insignificant to identify the crack location.

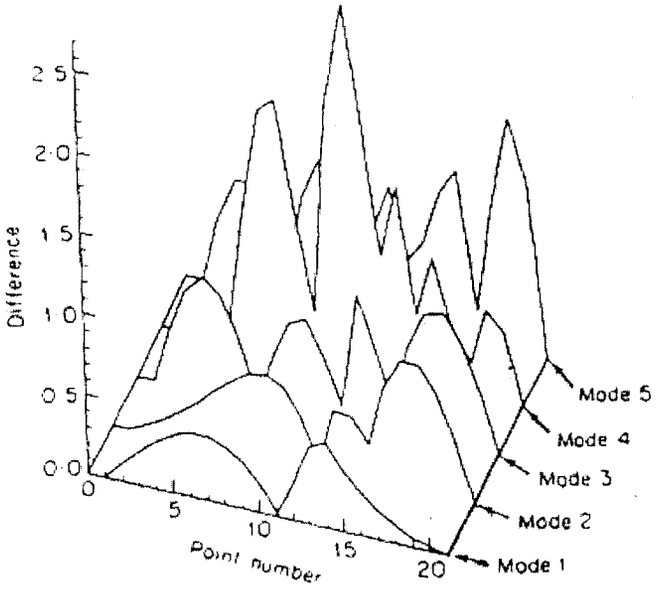

Figure 2.6 Absolute deviations in displacement mode shapes between the intact and damaged (element 13 with 50% reduction in E) simply supported beam [12]

2.3.4.2 CURVATURE MODE SHAPE

Curvature mode shape is related to the flexural stiffness of the beam's cross section. Curvature at a point is given by

$$v'' = M/(EI) \qquad \text{Equation 2.36}$$

in which v'' is the curvature of the section and M its bending moment. Curvature is also proportional to the bending strain at the section.

$$\varepsilon = y/R = yv'' \qquad \text{Equation 2.37}$$

where ε is strain of the section and R is the radius of the curvature at the section.

When there is a crack or other damages in a structure, bending stiffness (EI) of the structure at the crack section or in the damaged region reduces, increasing the magnitude of curvature at that section of the structure. The changes in curvature are local in nature and hence can be used to detect and locate a crack or damage in the structure. Theoretically, the magnitude of change in curvature is inversely proportional to the value of EI.

Pandey [12] introduced a new parameter called curvature mode shape for identifying and locating damage in a structure. In his investigation, only the translation degree of freedom along Y axis (vertical direction) was considered in the analysis. This was done because in any experimental work, rotations are not generally measured because of difficulty in their measurement. Moreover, since the main interest is in the flexural modes of vibration, translation along the X axis can be neglected.

The displacement mode shapes obtained from a FEM simply supported beam were used to calculate curvature mode shapes and they were obtained numerically by using a central difference approximation given as

$$v'' = (y_{n+1} - 2y_n + y_{n-1})/h^2 \qquad \text{Equation 2.38}$$

where h is the length of the elements and y_n is the displacement mode shape at n node. The absolute difference between the curvature mode shapes of the intact and the damaged case were plotted and shown in Figure 2.7. The maximum difference for every curvature mode shape occurs in the damaged zone located at 13th element. These numerical results demonstrate the effectiveness of curvature mode shapes in detecting and locating a state of damage. This indicates that the changes in curvature mode shapes are localized in the region of damage.

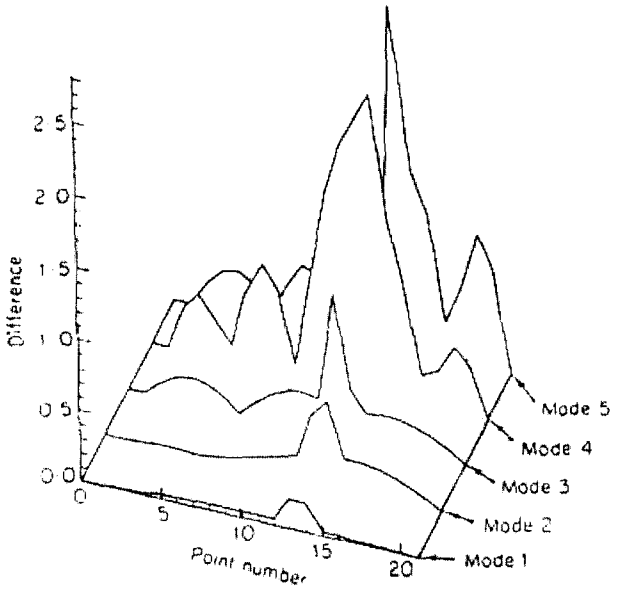

Figure 2.7 Absolute differences between curvature mode shapes for the intact and damaged (element 13 with 50% reduction in E) simply supported beam. [12]

Ratcliffe [13] also used a similar approach and applied a finite difference approximation of Laplace's differential operator [24] to the displacement mode shapes. This operator, as given in Equation 2.39, was successfully applied to the numerical data obtained from experimental and FE modeling of a free-free uniform beam.

$$L_n = (y_{n+1} - 2y_n + y_{n-1}) \qquad \text{equation 2.39}$$

Figure 2.8(a) shows the method being used for the first bending mode of finite element free-free beam with 50% damage between nodes 7 and 8. This level of damage is severe enough to cause a noticeable anomaly in the mode shape. However, with less severe damage, the Laplacian retained its characteristic shape, with less pronounced effects. This is shown, for 5% damage to the same beam, in Figure 2.8(b). The Laplacian had a similar shape and identifies damage in a similar fashion to the curvature mode shapes in reference [12]. The main difference was that Pandey [12] considered the difference in curvature between undamaged and damaged beams, whereas the Laplacian only considered the damaged model.

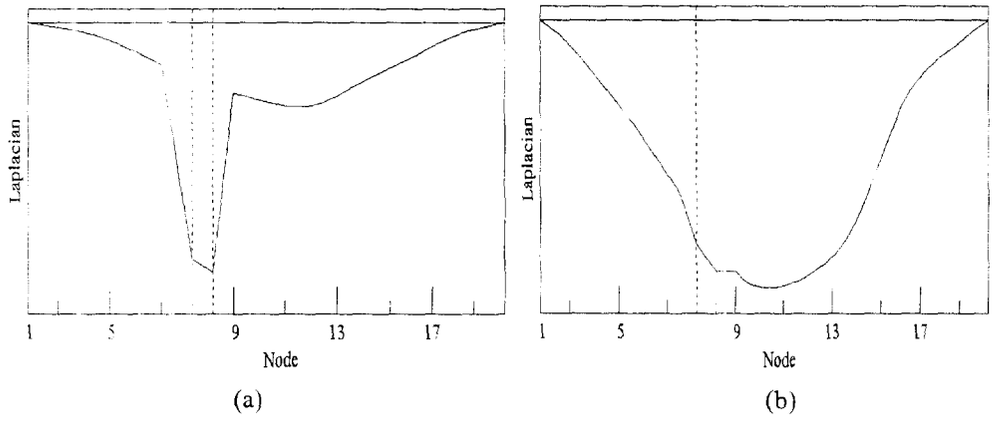

Figure 2.8 Laplacian for (a) 50% and (b) 5% [13]

In conclusion, curvature mode shape or the Laplacian method is a good indicator for identifying damage location but only applicable when the damage is severe. The mode shape data from the fundamental modes or lower modes are most suited to this technique. However, data obtained from higher modes are less sensitive and are particularly used to verify results from the fundamental modes.

2.3.5 MODAL ASSURANCE CRITERIA

Modal Assurance Criteria (MAC) [14] and Coordinate Modal Assurance Criteria (COMAC) [15] are commonly used to compare the difference between two sets of

vibration mode shapes. MAC indicates the correlation between two sets of mode shapes. It is used to study overall differences in the mode shapes, while COMAC indicates the correlation between the mode shapes at a selected measurement point of a structure and is used to compare mode shapes in a point-wise manner [12,16].

Pandey [12] used MAC and COMAC values for the intact and damaged displacement mode shapes to evaluate the state of health of a beam. The values of MAC and COMAC from the uniform cantilever beam and simply supported beam did not indicate any presence of damage by returning 100 percent compatibility. As concluded in the study, MAC and COMAC are not sensitive enough to detect damage at its earlier stages. The reason is that MAC is calculated based on the average differences over all the measurement points whereas COMAC is calculated based on the average differences over all the mode shapes [17].

Ndambi [38] carried out an investigation to evaluate the use of dynamic techniques for damage detection in reinforced concrete (RC) beams. The 6m RC beams were subjected to progressive cracking introduced at different load steps. The damaged sections were located in symmetrical or asymmetrical positions according to the applied load on the beams. A comparison of the set of measurements in damaged and undamaged states of the beams allowed the sensitivity analysis of natural frequency, MAC and COMAC to the crack damage in RC beams to be performed. Figure 2.9 shows the set up of symmetrical and asymmetrical loading configurations.

In the case of the symmetrical crack configuration, a decreasing tendency was observed in the MAC factors for each considered eigenmode. This decrease expressed the alteration of the RC beams by the decrease in the rigidity in certain zones of the structure. However, the decrease was inconsistent and made the interpretation of the obtained results more difficult. The inconsistent trend could be explained by the high

sensitivity of the MAC factors to measurement errors. Figure 2.10 shows the MAC factors as a function of the static symmetrical loading configuration.

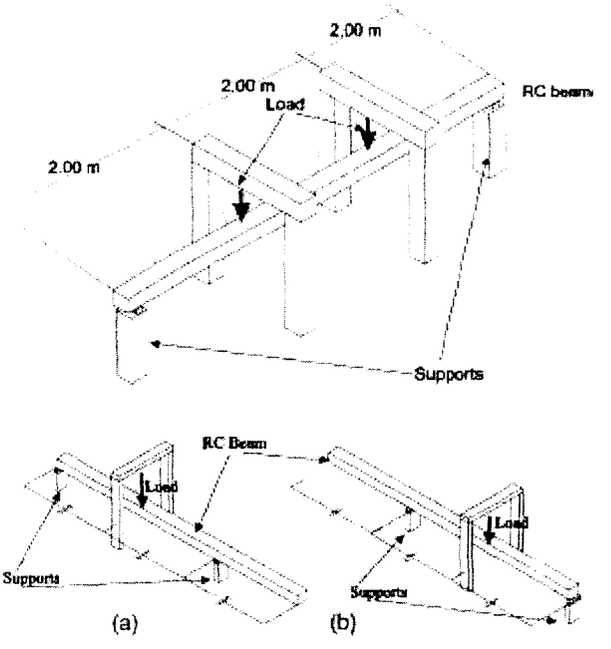

Figure 2.9 Static load test: symmetrical and asymmetrical loading configurations [38]

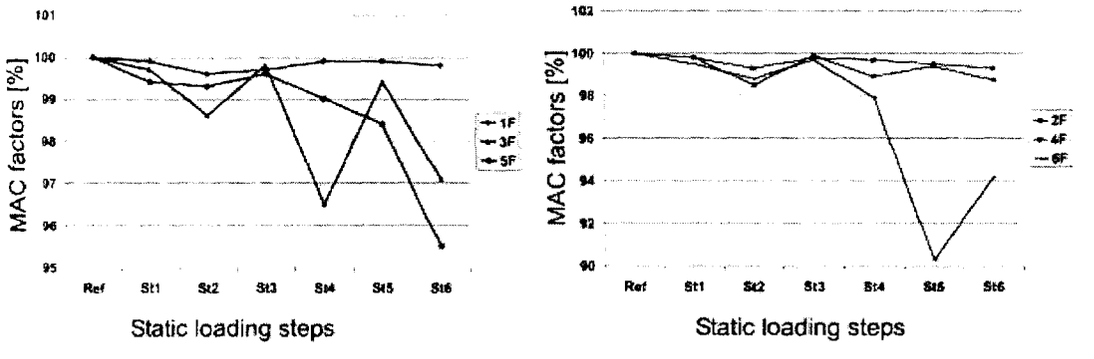

Figure 2.10 MAC for the symmetrical loading configuration [38]

The MAC factors in the case of the asymmetrical crack configuration decreased in the first set-up configuration (case 'a' of the asymmetrical configuration). The decrease was nearly consistent for each considered eigenmode indicating the alteration in rigidity of the structure. For case b, the results was in contrast with increase of the MAC factors as if the structure had been restored. From these results, it was concluded

that the asymmetrical crack damage occurring in the RC beam caused a decrease of the MAC factors expressing the asymmetrical alteration of the structure. Another conclusion was that a symmetrical damage occurring in a structure has less influence on the MAC factors than the asymmetrical one. Figure 2.11 shows the MAC factors for the static asymmetrical loading configuration.

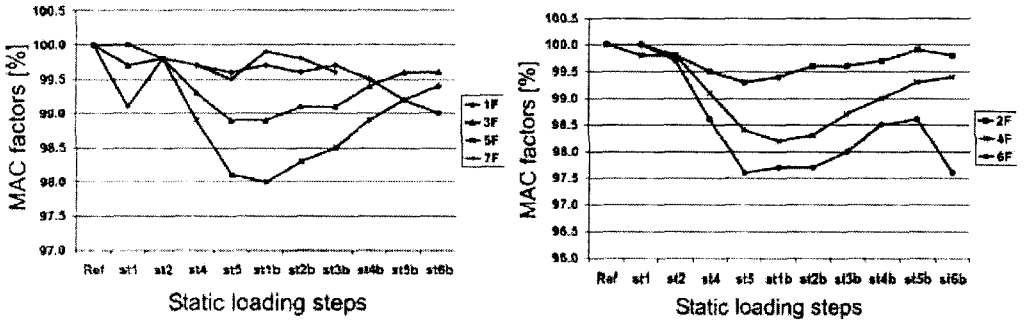

Figure 2.11 MAC for the asymmetrical loading configuration [38]

According to Ndambi [38], eigenfrequncies and MAC factors can only indicate whether damage exists. In practice, it is important to identify the damage location and to resolve this problem. The use of mode shape derivatives providing information for individual measurement points is adequate. The COMAC factor is a candidate for such a parameter. Referring to Figure 2.12, the trend of the subtracted values of the COMAC from unity (1-COMAC) for the symmetrical crack configuration shows a maximum drop ranging from 0.8 % to 15 % on points 11 and 21 where the static loading was applied. This was apparent in all the considered loading steps giving an indication of the damaged sections along the beam. Figure 2.12 shows the 1-COMAC as a function of measurement points for loading stage 1, stage 3, stage 5 and stage 6.

For the asymmetrical crack configuration, Figure 2.13 shows the 1-COMAC values for the case 'a' of the asymmetrical static loading configuration. Three static loading steps were presented as st1a, st2a and st5a. The maximum drop of the COMAC factor was of the order of 4.5 %, which was obtained after the final static loading step

st5a. This drop was situated at loading point 11 indicating the damaged section of the beam; on the other hand looking at Figure 2.14 corresponding to the case b, it was difficult to detect the new damaged section. The drop in COMAC remained located in the neighborhood of point 11. No indication was evident concerning the second damaged section corresponding to loading point 21. Ndambi [38] concluded that it was difficult to detect two different damaged sections in the same beam with different severity of damage. Figure 2.14 shows the 1-COMAC for stage 1b, 2b, 5b, and 7b.

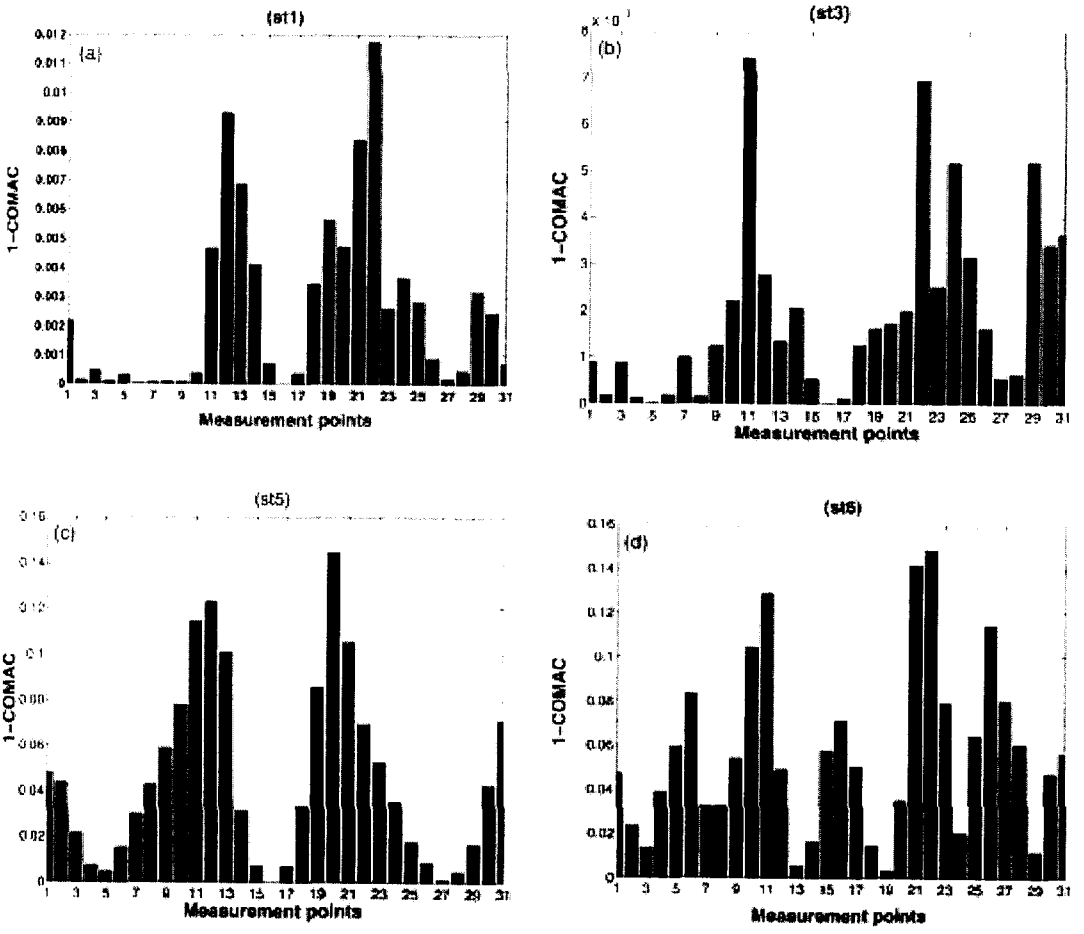

Figure 2.12 1 – COMAC in loading stage 1, stage 3, stage 5 and stage 6 [38]

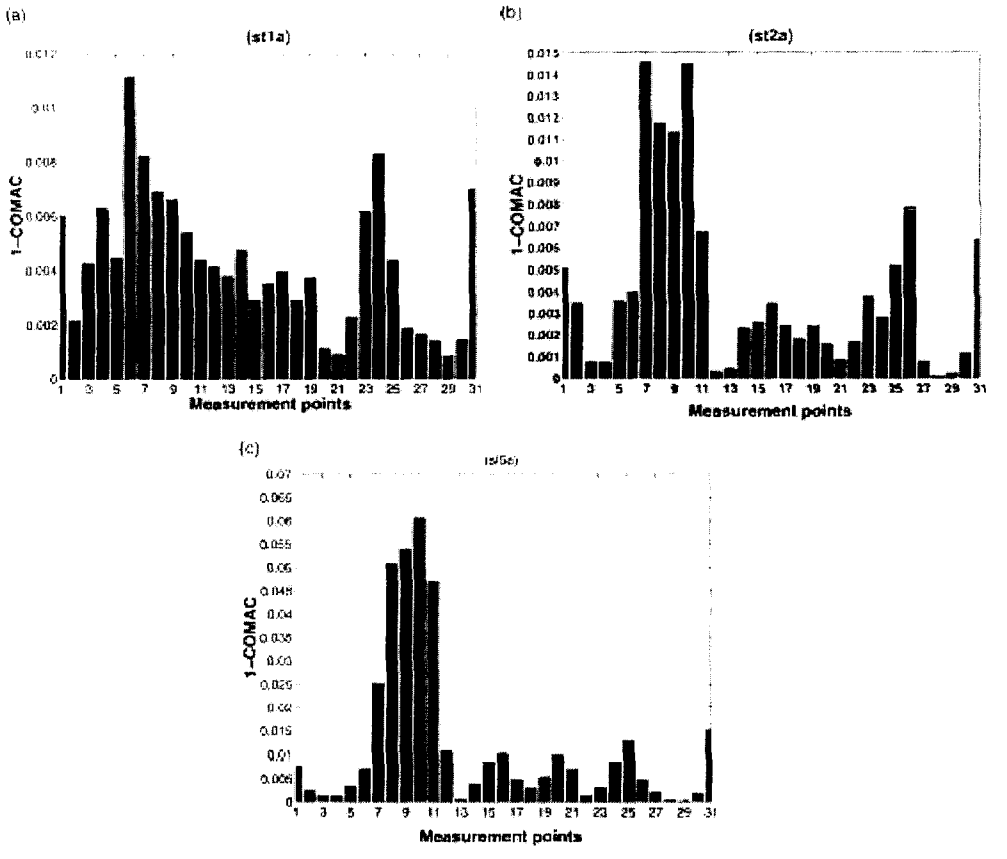

Figure 2.13 1 – COMAC loading case 'a' for stage 1, stage 2 and stage 5 [38]

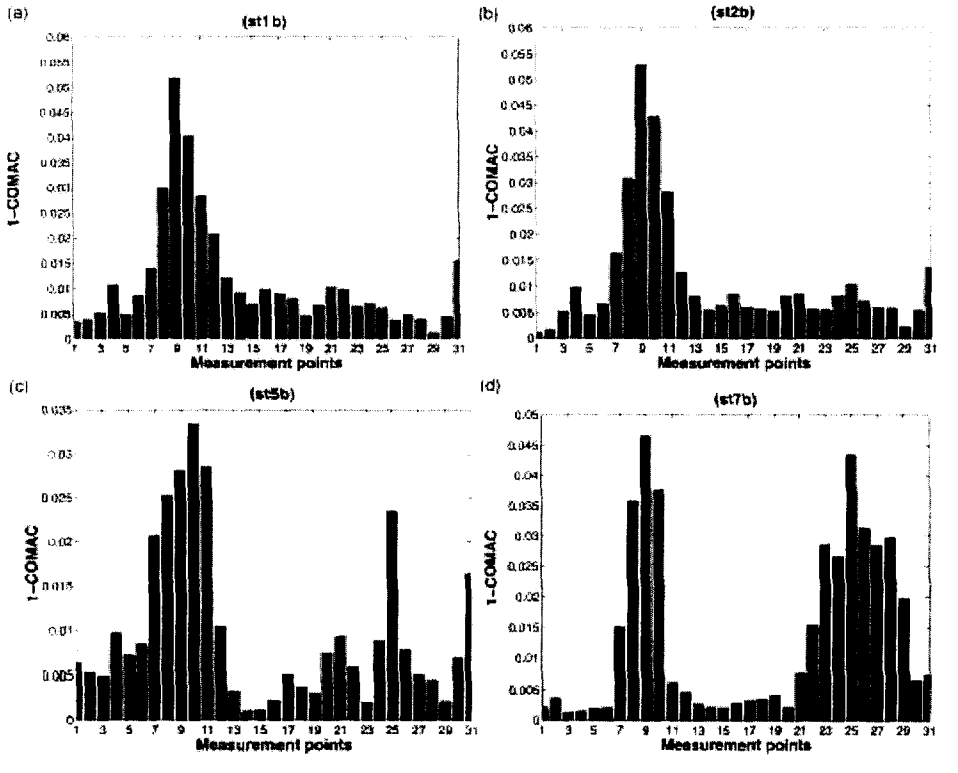

Figure 2.14 1 – COMAC loading case b for stage 1, stage 2, stage 5 and stage 7 [38]

2.4 MODEL UPDATING

The finite element (FE) model is commonly used in model updating technique. The FE model usually consists of numerous design parameters and updating the design parameters provides better correlation between FE analysis and experimental modal analysis. Ewins [18] suggested three steps for updating the model as listed below.

1 step: To make a direct and objective comparison of specific dynamic properties, measured versus predicted i.e. natural frequency and mode shape.

2 step: To quantify the extent of the differences or similarities between the two sets of data i.e. MAC and COMAC.

3 step: To make adjustments or modifications to one or another set of results in order to bring them closer into line with each other i.e least squares technique.

In this section, only step 1 and step 2 will be discussed.

2.4.1 NATURAL FREQUENCIES COMPARISON

Natural frequencies comparison between measured and predicted is often done by plotting experimental values against analytical values for all available modes or selected modes, as shown in Figure 2.15. It presents not only the degree of correlation between the two sets of results but also the nature of any discrepancies which exist [18]. The points obtained from the experimental and analytical results should lie on or close to, a straight line with a slope of unity, for perfectly correlated data, as shown in Figure 2.15. If the points are widely scattered about the line then there is poor correlation which is caused by some consistent error, for example, an erroneous material property used in the model.

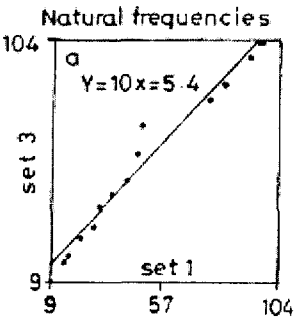

Figure 2.15 Plots of measured versus predicted natural frequencies [18]

Using only measured and predicted natural frequencies to correlate the two sets of data are not sufficient as there is no guarantee that measured modes correspond with their predicted counterparts. Therefore some positive identification of each mode with its counterpart is essential to provide a set of Correlated Mode Pairs (CMPs). The mode shape correlation methods are discussed in the next section.

2.4.2 MODE SHAPES COMPARISON

Mode shapes are unique which represent the motion of one point relative to another at resonance. Thus comparison of mode shapes should be made simultaneously with natural frequencies to ensure that the correlated mode pairs are correctly matched. Mode shapes can be compared either graphically or using numerical methods.

2.4.2.1 MODE SHAPES COMPARISON – GRAPHICAL

The most direct way to compare the mode shapes is by plotting the deformed shape for each model, namely experimental and predicted, and overlaying one plot on the other. Although this approach shows up differences, they are still difficult to interpret and the resulting plots become very confusing when involving too much information [18].

A more convenient approach in a similar fashion is by plotting experimental mode shapes against predicted ones, as shown in Figure 2.16. Perfectly correlated modes should have points lying close to a straight line of slope ±1.

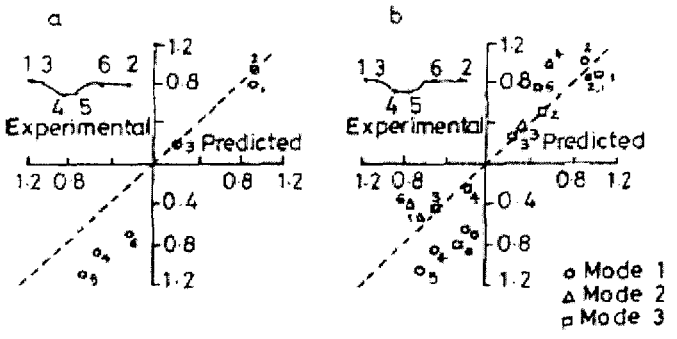

Figure 2.16 Plots of measured versus predicted mode shape vectors, (a) single mode; (b) 3 modes [18]

This approach can clearly interpret the cause of the discrepancy for two sets of mode shape data. If the points lie close to a straight line of slope significantly different from ±1, then either one or other mode shape is not mass-normalised or there is some other form of scaling error in the data. If the points are widely scattered about a line, then there is considerable inaccuracy in one or other set. If the points are scattered excessively, then it may be the case that the two eigenvectors whose elements are being compared do not relate to the same mode.

2.4.2.2 MODE SHAPES COMPARISON – NUMERICAL

The Modal Scale Factor (MSF) is represented by the 'slope' of the best straight line through the points as plotted in Figure 2.16. This quantity is defined as

$$MSF(X,A) = \frac{\sum_{j=1}^{n} \phi_{Xj}\phi_{Aj}^{*}}{\sum_{j=1}^{n} \phi_{Aj}\phi_{Aj}^{*}}$$

or expressed alternatively as

$$MSF(A,X) = \frac{\sum_{j=1}^{n} \phi_{Xj}\phi_{Aj}^{*}}{\sum_{j=1}^{n} \phi_{Xj}\phi_{Xj}^{*}} \qquad \text{Equation 2.40}$$

However, the MSF gives no indication as to the quality of correlation by simply computing its slope. Therefore Mode Shape Correlation Coefficient (MSCC) or more popularly Modal Assurance Criterion (MAC) is used to provide a better indication of correlation. MAC is a measurement of the least-squares deviation of the points from the straight line correlation and defined as

$$MAC(A,X) = \frac{\left|\sum_{j=1}^{n} \phi_{Xj}\phi_{Aj}^{*}\right|^{2}}{\left(\sum_{j=1}^{n} \phi_{Xj}\phi_{Xj}^{*}\right)\left(\sum_{j=1}^{n} \phi_{Aj}\phi_{Aj}^{*}\right)} \qquad \text{Equation 2.41}$$

The MAC value close to 1 suggests that the two modes are well correlated and a value close to 0 indicates uncorrelated modes.

In the above calculation, MAC and MSF only indicate a correlation between two sets of mode shapes but not that between the mode shapes at a selected measurement point or node on the structure. The Coordinate Modal Assurance Criterion (COMAC) proposed by Lieven and Ewins in 1988 [15] defined as

$$COMAC(A_i,X_i) = \frac{\sum_{l=1}^{L} \left|\phi_{Xil}\phi_{Ail}\right|^{2}}{\left(\sum_{l=1}^{L} \phi_{Xil}^{2}\right)\left(\sum_{l=1}^{L} \phi_{Ail}^{2}\right)} \qquad \text{Equation 2.42}$$

where l represents an individual correlated mode pair at i node and L is the total number of correlated mode pairs. A COMAC value close to 1 indicates a good correlation at the selected location between the two sets of data. On the other hand, a low COMAC value indicates the discrepancies at that particular region.